Study of Galaxy Collisions and Thermodynamic Evolution of Gas Using the Exact Integration Scheme

Koki Otaki[1,2(✉)] and Masao Mori[3]

[1] Degree Programs in Pure and Applied Sciences, Graduate School of Science and Technology, University of Tsukuba, Tennodai 1-1-1, Tsukuba, Ibaraki 305-8577, Japan
otaki@ccs.tsukuba.ac.jp

[2] Degree Programs in Systems and Information Engineering, Graduate School of Science and Technology, University of Tsukuba, Tennodai 1-1-1, Tsukuba, Ibaraki 305-8577, Japan

[3] Center for Computational Sciences, University of Tsukuba, Tennodai 1-1-1, Tsukuba, Ibaraki 305-8577, Japan
mmori@ccs.tsukuba.ac.jp

Abstract. Radiative cooling of the interstellar medium plays a vital role in the context of galaxy formation and evolution. On the other hand, the cooling time in the high-density regions involving star formation is much shorter than the dynamical time of the gas. In numerical simulations, it is challenging to solve physical phenomena coexisting on significantly different timescales, and it is known as the overcooling problem in the study of galaxy formation. Townsend (2009) has developed the Exact Integration (EI) scheme that provides a stable solution for the cooling term in the energy equation of astrophysical fluid dynamics, regardless of the size of the simulation time step. We apply the EI scheme to define the effective cooling time that accounts for the temperature dependence of the cooling rate and investigate the thermodynamic evolution of gas in colliding dark matter subhalos. The results show that the conventional cooling time always indicates a shorter than the effective cooling time derived by the EI scheme because it does not include the dependence of the cooling rate on temperature. Furthermore, we run three-dimensional galaxy collision simulations to examine the difference in thermodynamic evolution between the EI scheme and the conventional Crank–Nicholson method for solving the cooling equation. Comparing the results of the two simulations, we find that the EI scheme suppresses the rapid temperature decrease after galaxy collisions. Thus, the EI scheme indicates considerable potential for solving the overcooling problem in the study of galaxy formation.

Keywords: Galaxies · Evolution · Galaxies · Interactions · Methods · Numerical

© The Author(s) 2022
O. Gervasi et al. (Eds.): ICCSA 2022 Workshops, LNCS 13378, pp. 373–387, 2022.
https://doi.org/10.1007/978-3-031-10562-3_27

1 Introduction

In the standard galaxy formation model, it is believed that cold dark matter (CDM) drives a hierarchical structure formation in the universe. Based on the CDM model, small structures grow up to larger structures through repeated collisions and merges. The gas falls into the deep gravitational potential well created by the dark matter halo, where stars and galaxies are formed. Radiative cooling is an essential physical process in galaxy formation since stars form in dense regions of gravitational contraction triggered by gas energy loss. The cooling time in the high-density regions where star formation occurs is much shorter than the dynamical time. It is a hard problem to solve physical phenomena with significantly different timescales. Supernova explosion significantly affects the evolution of the galaxy and suppresses star formation since it ejects a large amount of energy into the surrounding gaseous medium. However, in simulations of galaxy formation, it is difficult to capture the effects of supernova energy feedback because most of the energy is lost through radiative cooling. The problem of too short a cooling time to simulate physical phenomena in the simulations is known as the overcooling problem. Typically, the implicit integration method is used to handle time steps longer than the cooling time in the simulations. However, this method may estimate inadequate solutions due to multiple roots.

Townsend [19] has developed the Exact Integration (EI) to solve the cooling term of the energy equation stably regardless of the size of the simulation time step. This scheme provides temperatures by using a temporal evolution function given a cooling rate fitted by a piecewise power law, which accounts for the temperature dependence of the cooling rate. Zhu et al. [22] have applied this scheme to cosmological simulations and showed that it is closer to the equilibrium state where radiative cooling balances the heating effect of the ultraviolet background compared to previous simulations. This study defines the effective cooling time by adopting the EI scheme. We then estimate and compare gas timescales using an analytical model of dark matter subhalo collisions in Sect. 2. In Sect. 3, we run three-dimensional simulations of dark matter subhalo collision and discuss the differences of the thermodynamic evolution in the EI scheme and the Crank–Nicholson scheme, respectively.

2 Simple Model for Colliding Homogeneous Gas

Galaxy collision events are different from the standard evolution of isolated galaxies as the shock waves generated at the collision surface have a significant impact on the thermodynamic evolution. We focus on the head-on collisions between two dark matter subhalos (DMSHs) in the massive dark matter halo to evaluate the thermodynamic evolution of gas and timescales of physical processes. A DMSH consists of gas and dark matter components and is assumed to have a dark matter mass to gas mass ratio of 5.36. We consider a collision between two gas clouds in each DMSH as a simple one-dimensional (1D) model and assume that two colliding clouds both have mass $M_{\rm gas}$, uniform density ρ_0

within scale radius r_s. For simplicity, initial pressure and specific internal energy are zero, $p_0 = u_0 = 0$. The centres of the cloud are initially at $x = \pm r_s$, and the bulk-velocities are $\mp v_{col}$, respectively (Fig. 1). The subscript 0 indicates the physical quantities before the collision of the DMSHs, and the subscript 1 indicates the physical quantities after the shock wave generated by the collision has passed through.

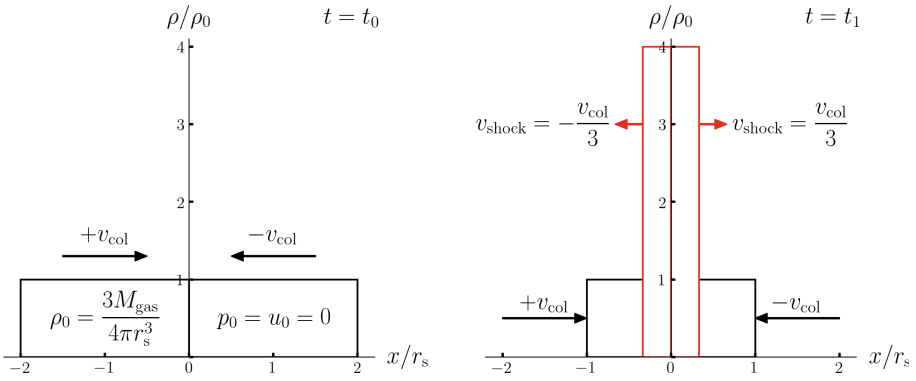

Fig. 1. 1D analytical model of hydrodynamics. Left panel: the gas density before the collision. Right panel: the gas density after the collision.

The density of the shocked clouds according to the Rankine-Hugoniot (RH) condition for strong adiabatic shocks are

$$\rho_1 = \frac{\gamma + 1}{\gamma - 1}\rho_0, \tag{1}$$

where γ is the specific heat ratio. We have used $\gamma = 5/3$. Assuming that the system's kinetic energy is converted into thermal energy as $u_1 = v_{col}^2/2$, we can derive the shock velocity using RH condition for the conservation of mass,

$$v_{shock} = \frac{1}{3}v_{col}. \tag{2}$$

When the shock waves reach their cloud surface, shock-breakout ejects most of the gas from the system. The shock-crossing time is given by

$$t_{cross} = \frac{2r_s}{v_{col} + v_{shock}}. \tag{3}$$

We compare it with other timescales such as the free-fall time and cooling time to evaluate the thermodynamic evolution. The gravitational free-fall time in the shocked gaseous medium is

$$t_{ff} = \sqrt{\frac{3\pi}{32G\rho_1}}, \tag{4}$$

where G is the gravitational constant. The conventional cooling time in the shocked gaseous medium is

$$t_{\rm cool,conv} = \frac{k_{\rm B} m_{\rm p} \mu_1 T_1}{(\gamma - 1)\rho_1 \Lambda_1}, \tag{5}$$

where $k_{\rm B}$ is the Boltzmann constant, $m_{\rm p}$ is the atomic mass, T is the temperature, $\mu = \mu(T)$ is the molecular weight and $\Lambda = \Lambda(T)$ is the cooling rate. The internal energy u and the temperature T are related to the equation of state of ideal gas:

$$T = \frac{(\gamma - 1)\mu m_{\rm p} u}{k_{\rm B}}. \tag{6}$$

We assume that the gas has the solar metal abundance and is under the collisional ionization equilibrium. `MAPPINGS V` [17,18] code is adopted to calculate the molecular weight and the cooling rate (Fig. 2).

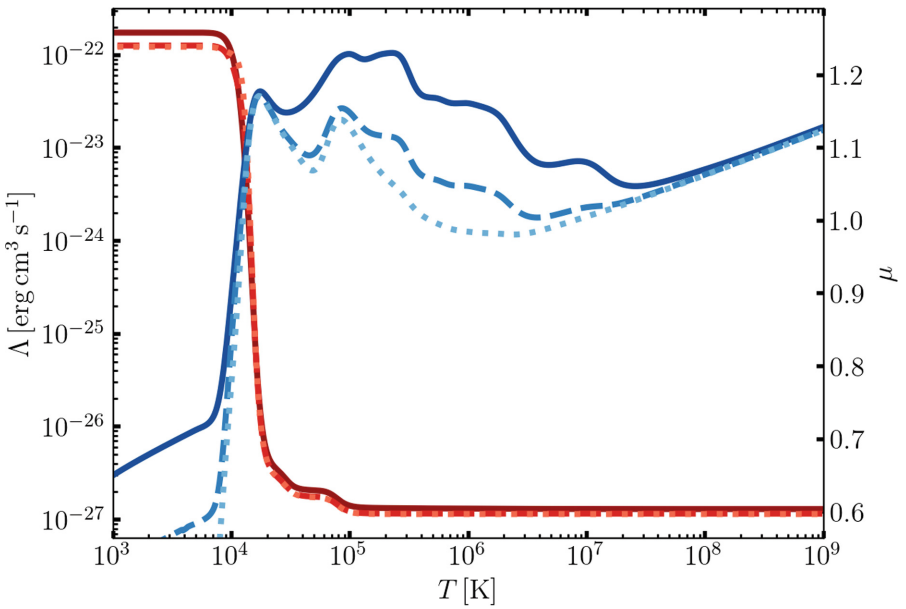

Fig. 2. Cooling rate Λ (blue) and mean molecular weight μ (red) for gas assuming the collisional ionisation equilibrium. The solid, dashed and dotted lines correspond to the gas metallicity of $1\,{\rm Z}_\odot$, $0.1\,{\rm Z}_\odot$ and $0.01\,{\rm Z}_\odot$, respectively. The metallicity refers to the abundance of elements heavier than helium, and $\rm Z_\odot$ represents the metal abundance in the Sun. (Color figure online)

Here, in order to consider the thermodynamic evolution of the gas in DMSH collision, we then define the effective cooling time based on the feature that

the EI scheme provides the exact temperature change. The cooling term of the energy equation is expressed as

$$\frac{\mathrm{d}T}{\mathrm{d}t} = -\frac{(\gamma-1)\rho\Lambda}{k_{\mathrm{B}}m_{\mathrm{p}}\mu}, \tag{7}$$

and to integrate it, the temporal evolution function (TEF) is defined as

$$Y_T(T) \equiv \frac{\Lambda_{\mathrm{ref}}}{\mu_{\mathrm{ref}}T_{\mathrm{ref}}}\int_T^{T_{\mathrm{ref}}}\frac{\mu}{\Lambda}\mathrm{d}T, \tag{8}$$

where the subscript "ref" means an arbitrary reference value in the EI scheme. We also take into account the time evolution of the mean molecular weight. $Y_T(T)$ can be calculated analytically as a table by fitting the cooling function Λ with a piecewise power-law. Using the TEF, we integrate Eq. (7) from the temperature T_{start} to cooled temperature T_{end} and define the effective cooling time,

$$t_{\mathrm{cool,\,eff}}(T_{\mathrm{start}} \to T_{\mathrm{end}}) \equiv [Y_T(T_{\mathrm{end}}) - Y_T(T_{\mathrm{start}})]\,\frac{k_{\mathrm{B}}m_{\mathrm{p}}}{(\gamma-1)\rho}\,\frac{\mu_{\mathrm{ref}}T_{\mathrm{ref}}}{\Lambda_{\mathrm{ref}}}. \tag{9}$$

If we set $T_{\mathrm{ref}} = T_{\mathrm{start}}$, the effective cooling time is expressed as

$$t_{\mathrm{cool,\,eff}}(T_{\mathrm{start}} \to T_{\mathrm{end}}) = Y_T(T_{\mathrm{end}}) \times t_{\mathrm{cool,\,conv}}(T_{\mathrm{start}}). \tag{10}$$

Hence, it can be understood that Y_T acts as a correction factor in the relationship between the effective cooling time and the conventional cooling time.

The timescales of each physical process as a function of collision velocity are shown in Fig. 3. Assuming that the kinetic energy of the collision velocity is fully converted to internal energy, the timescales are represented as a function of the temperature of the gas after the collision. In the DMSHs collision with a collision velocity of $100\,\mathrm{km\,s^{-1}}$, the cooling times are shorter than the shock-crossing time and the free-fall time. The conventional cooling time for $2.4\times10^5\,\mathrm{K}$ corresponding to the collision velocity of $100\,\mathrm{km\,s^{-1}}$ is about 0.02 Myr. On the other hand, the effective cooling time for decreasing from $2.4\times10^5\,\mathrm{K}$ to $10^4\,\mathrm{K}$ is about 0.07 Myr, but the effective cooling time for $T_{\mathrm{end}} = 10^3\,\mathrm{K}$ is 10 Myr. The conventional definition estimates a shorter cooling time than the new definition because of the temperature dependence of the cooling rate. Thus, it is found that there is a decisive difference between the conventional method and the present method and that it is quite effective to employ the present method in order to track accurate radiative cooling in the study of galaxy formation.

3 Three-Dimensional Model for Colliding Gas Spheres

In the previous section, we presented a physical insight into the collision process of DMSHs using an analytical model. However, this analytical model contains several uncertain assumptions. For instance, it is easy to foresee that the uniformity of the system is severely violated in an actual situation, and the inhomogeneity of the density field makes further nonlinear evolution of the gaseous system. In this section, we perform three-dimensional collision simulations of DMSHs to study the evolution of gas.

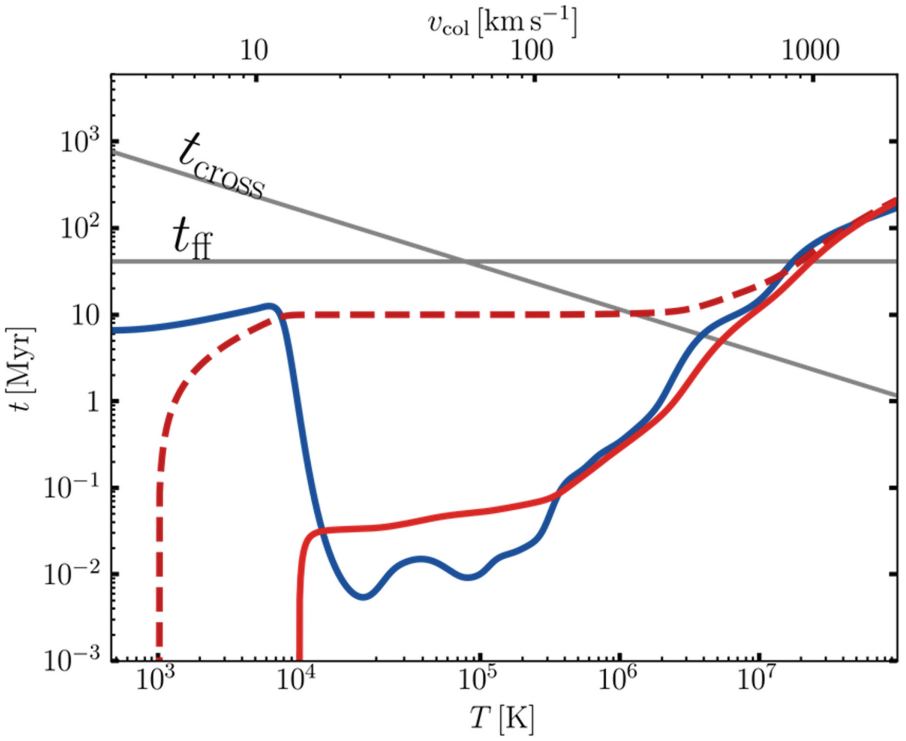

Fig. 3. Timescales after gas collisions. The temperature is calculated using the assumption that the kinetic energy is fully converted to internal energy. The blue line is the conventional cooling time $t_{\rm cool,\,conv}(T)$. The red lines are the effective cooling time $t_{\rm cool,\,eff}(T \to T_{\rm end})$, with the solid line corresponding to the timescale for $T_{\rm end} = 10^4$ K, and the dashed line corresponding to the timescale for $T_{\rm end} = 10^3$ K. The two gray lines are the shock-crossing time $t_{\rm cross}$ and free-fall time $t_{\rm ff}$, respectively. (Color figure online)

3.1 Model Description

The simulations of DMSHs collision are performed with the N-body/Smoothed Particle Hydrodynamics (SPH) [6,8] code implemented for this study. This code is parallelized by the Framework for Developing Particle Simulators (`FDPS`) [7,11]. It includes functions such as domain decomposition, redistribution of particles, and gathering of particle information for interaction calculation. The `FDPS` libraries are implemented using OpenMP for intra-node parallelism and MPI for inter-node parallelism. Using these libraries, users can easily implement parallelized programs by writing sequential code for interaction calculations. We use C++ bindings of `FDPS`. The gravitational forces are calculated with a tree algorithm [2,3] and the tree-opening angle is 0.7.

In the SPH formulation, the gas density of one particle at position $\boldsymbol{r}_i$ is given by

$$\rho_i = \sum_{j=1}^{N_{\rm neigh}} m_j W(r_{ij}, h_i), \tag{11}$$

where m_j is the mass of gas particle at $\boldsymbol{r}_j$, $r_{ij} = |\boldsymbol{r}_i - \boldsymbol{r}_j|$, $W(r,h)$ is the smoothing kernel, h is the smoothing length and $N_{\rm neigh} = 200$ is the number of neighbour particles. For the kernel function, we adopt the Wendland C^4 function [20],

$$W(r,h) = \frac{495}{32\pi h^3} \begin{cases} (1-q)^6(1+6q+\frac{35}{3}q^2), & q \le 1, \\ 0, & q > 1, \end{cases} \tag{12}$$

where $q = r/h$, to avoid the clumping instability [4,21]. We followed the formulation of SPH introduced by [16]. The smoothing length h_i of each particle is determined by

$$\frac{4\pi}{3} h_i^3 \rho_i = \overline{m} N_{\rm neigh}, \tag{13}$$

where $\overline{m}$ is an average mass of gas particles. These Eqs. (11) and (13) need to be solved implicitly for ρ_i and h_i. However, the minimum value of smoothing length h is set to gravitational softening ϵ in order to match the spatial resolution.

The momentum equations for the gas particles are given by

$$\frac{{\rm d}\boldsymbol{v}_i}{{\rm d}t} = -\sum_j m_j \left[f_i \frac{p_i}{\rho_i^2} \nabla_i W(r_{ij}, h_i) + f_j \frac{p_j}{\rho_j^2} \nabla_i W(r_{ij}, h_j) + \Pi_{ij} \nabla_i \overline{W}_{ij} \right] \tag{14}$$

where $\boldsymbol{v}_i$, and p_i are the velocity and pressure of gas particle respectively, f_i is defined by

$$f_i = \left(1 + \frac{h_i}{3\rho_i} \frac{\partial \rho_i}{\partial h_i} \right)^{-1}, \tag{15}$$

and $\overline{W}_{ij}$ is a symmetrized kernel,

$$\overline{W}_{ij} = \frac{1}{2} \left[W(r_{ij}, h_i) + W(r_{ij}, h_j) \right]. \tag{16}$$

The artificial viscosity Π_{ij} needs to treat shocks. We adopt Monaghan's [10] artificial viscosity combined with Balsara's [1] switch (see Otaki & Mori [14]). The entropy $A_i = p_i/\rho_i^\gamma$ is conserved in adiabatic flow, but it is generated by artificial viscosity via shocks. The entropy equations are given by

$$\frac{{\rm d}A_i}{{\rm d}t} = \frac{1}{2} \frac{\gamma - 1}{\rho_i^{\gamma-1}} \sum_j m_j \Pi_{ij} \boldsymbol{v}_{ij} \cdot \nabla_i \overline{W}_{ij}, \tag{17}$$

where $A_i = p_i/\rho_i^\gamma$ is the entropic function for specific entropy.

In the dissipationless case, we solve only Eq. (17) for the thermal evolution, but since radiative cooling is important in galaxy formation, it is needed to add a dissipation term to the entropy equation:

$$\left(\frac{\mathrm{d}A}{\mathrm{d}t}\right)_{\mathrm{cool}} = \frac{\gamma - 1}{\rho^{\gamma}} \left(\frac{\mathrm{d}u}{\mathrm{d}t}\right)_{\mathrm{cool}} \tag{18}$$

where

$$\left(\frac{\mathrm{d}u}{\mathrm{d}t}\right)_{\mathrm{cool}} = -\frac{n^2 \Lambda(u, Z)}{\rho} = -\frac{\rho \Lambda(u, Z)}{\mu^2 m_{\mathrm{p}}^2}, \tag{19}$$

where n, μ and m_{p} are the number density of the gas, the mean molecular weight and the proton mass, respectively. Λ is the cooling function of the specific internal energy u and the metallicity Z. To compare the results of different methods of solving the cooling equation (19), we implement the EI scheme [19] and the Crank–Nicholson scheme.

For EI scheme, to integrate from time t^n to $t^{n+1} = t^n + \Delta t$ for each gas particle i, the Eq. (19) becomes

$$\int_{u_i^n}^{u_i^{n+1}} \frac{\mu(u)^2}{\Lambda(u, Z)} \mathrm{d}u = -\frac{\rho_i}{m_{\mathrm{p}}^2} \Delta t, \tag{20}$$

where $u_i^n = u_i(t^n)$ and $u_i^{n+1} = u_i(t^{n+1})$. Then, using the temporal evolution function defined by

$$Y_u(u) = \frac{\Lambda_{\mathrm{ref}}}{\mu_{\mathrm{ref}}^2 u_{\mathrm{ref}}} \int_u^{u_{\mathrm{ref}}} \frac{\mu(u)^2}{\Lambda(u, Z)} \mathrm{d}u, \tag{21}$$

the specific internal energy at the next time step is expressed by

$$u_i^{n+1} = Y_u^{-1} \left[Y_u(u_i^n) + \frac{\Lambda_{\mathrm{ref}}}{\mu_{\mathrm{ref}}^2 u_{\mathrm{ref}}} \frac{\rho_i}{m_{\mathrm{p}}^2} \Delta t \right]. \tag{22}$$

$Y_u(u)$ is the function corresponding to $Y_T(T)$, which is the result of the transformation using Eq. (6). It can be obtained as a table by fitting the cooling function Λ with a piecewise power-law. By using this integrated function $Y(u)$, the time evolution equation can be solved taking into account the temperature dependence of the cooling rate and is not sensitive to the size of the time step.

On the other hand, to solve the Eq. (19) with the Crank–Nicholson method,

$$u_i^{n+1} = u_i^n - \frac{1}{2} \left(\frac{\Lambda(u^{n+1})}{\mu(u^{n+1})^2} + \frac{\Lambda(u^n)}{\mu(u^n)^2} \right) \frac{\rho_i}{m_{\mathrm{p}}^2} \Delta t, \tag{23}$$

we calculate it using the bisection method.

The simulation time steps Δt share the same value throughout the system. It is determined by the CFL conditions:

$$\Delta t = \min_i(\Delta t_{i,\mathrm{grav}},\ \Delta t_{i,\mathrm{hydro}}), \tag{24}$$

$$\Delta t_{i,\mathrm{grav}} = C_{\mathrm{CFL}}\sqrt{\frac{\epsilon}{|\mathrm{d}\boldsymbol{v}_i/\mathrm{d}t|}}, \tag{25}$$

$$\Delta t_{i,\mathrm{hydro}} = C_{\mathrm{CFL}}\frac{h_i}{\max_j(v_{ij}^{\mathrm{sig}})}, \tag{26}$$

where C_{CFL} is the CFL constant and we set $C_{\mathrm{CFL}} = 0.3$. We adopted the second-order Runge–Kutta method for the time integration.

3.2 Thermodynamic Evolution of Colliding Gas

In order to study the physics of DMSH collisions, we have set up an ideal situation for a head-on collision. The two colliding DMSHs both have mass $M_{\mathrm{tot}} = M_{\mathrm{DM}} + M_{\mathrm{gas}} = 10^9\,\mathrm{M}_\odot$, the mass ratio between dark matter and gas is 5.36. A DMSH contains no stellar components.

The DMSH centres are initially at

$$(x,\ y,\ z) = (\pm 5,\ 0,\ 0)\,\mathrm{kpc}, \tag{27}$$

and the initial bulk velocities of the DMSHs are

$$(v_x,\ v_y,\ v_z) = (\mp 100,\ 0,\ 0)\,\mathrm{km\,s^{-1}}, \tag{28}$$

respectively. The density distribution of dark matter is the NFW profile [12, 13]. The gas is assumed under the hydrostatic equilibrium in the gravitational potential of the dark matter halo,

$$\rho_{\mathrm{gas}}(r) = \rho_{\mathrm{gas},0}\exp\left[-\frac{\mu m_{\mathrm{p}}}{k_{\mathrm{B}}T_{\mathrm{vir}}}\Phi_{\mathrm{NFW}}(r)\right], \tag{29}$$

where Φ_{NFW} is the gravitational potential of NFW profile and T_{vir} is the virial temperature of DMSH defined as

$$T_{\mathrm{vir}} = \frac{c(c^2 + 2c - 2(1+c)\ln(1+c))}{2((1+c)\ln(1+c) - c)^2}\frac{GM_{\mathrm{tot}}\mu m_{\mathrm{p}}}{3k_{\mathrm{B}}R_{200}}, \tag{30}$$

where $c = R_{200}/r_{\mathrm{s}}$ is a concentration parameter [15] and R_{200} is the radius that the average density of the DMSH is 200 times the critical density of the universe. To generate the initial conditions of a DMSH, we use the `MAGI` [9]. After generating particle distributions using `MAGI`, we calculated a DMSH for several hundred million years in an isolated system of adiabatic processes to suppress density fluctuations and reach dynamical equilibrium. We use 1.36 million particles in each simulation. The mass resolution of N-body particles and SPH particles is $\sim 10^3\,\mathrm{M}_\odot$, and all particles have the same mass. The spatial resolution is 100 pc.

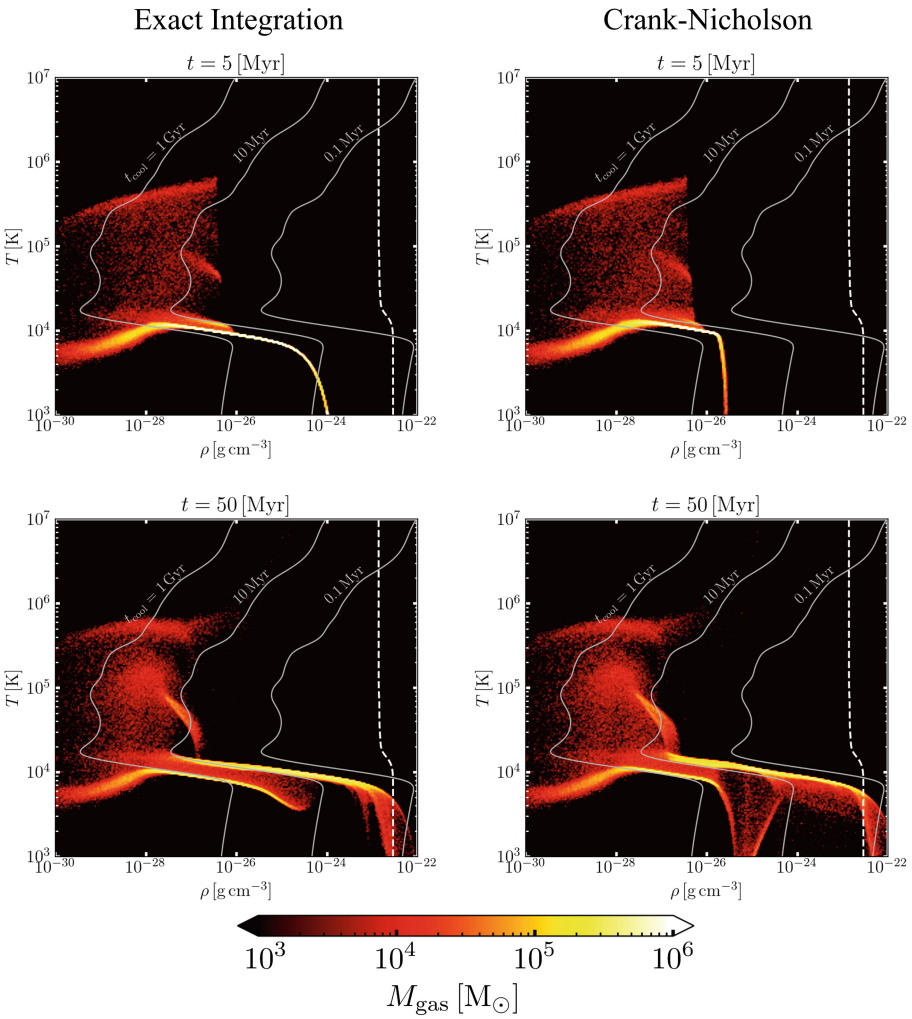

Fig. 4. Density-Temperature phase diagram for gas in the simulation box. The two left panels show the result of a simulation using the EI scheme at 5 Myr (upper panel) and 50 Myr (lower panel). The two right panels show the result of a simulation using the Crank–Nicholson scheme at 5 Myr (upper panel) and 50 Myr (lower panel). The white dashed line is a number density of $10\,\mathrm{cm}^{-3}$. The white solid lines represent the cooling time calculated by the conventional definition.

The cooling rate for gas with a metallicity of $1\,\mathrm{Z}_\odot$ is calculated by `MAPPINGS V` [17,18] assuming the collisional ionisation equilibrium.

Figure 4 shows the resultant gas distributions on the density-temperature plane for collision simulations using the EI scheme and the Crank–Nicholson scheme, respectively. The upper left and lower left panels in Fig. 4 show the

thermodynamic evolution using the EI scheme, at 5 Myr and 50 Myr from the initial condition, respectively. On the other hand, the two panels on the right in Fig. 4 indicate the simulation results solved using the Crank–Nicholson scheme. The white solid lines are the conventional cooling time and the white dashed line indicate a number density of $10\,\mathrm{cm}^{-3}$.

At 5 Myr, the temperature increases to $\sim 10^{5-6}$ K in the low-density region due to collisions in between the outside of the DMSHs. At the same time, in the high-density region at the centre of the DMSHs, the temperature suddenly decreases due to radiative cooling. Comparing the two schemes, the EI scheme has gas with 10^4 K and $10^{-25}\,\mathrm{g\,cm}^{-3}$, whereas the Crank–Nicholson scheme indicates that most of the gas denser than about $10^{-26}\,\mathrm{g\,cm}^{-3}$ have the temperature lower than 10^4 K. The conventional cooling time for the gas with $\sim 10^{-25}\,\mathrm{g\,cm}^{-3}$ and $\sim 10^4$ K is enough longer then 5 Myr, suggesting that the Crank–Nicholson scheme estimates a larger amount of energy loss.

The temperature distribution in the high-density regions is completely different between the two schemes at 50 Myr, when the centre of the two DMSHs collide. The Crank–Nicholson scheme overestimates the cooling efficiency. Therefore, the temperature drops rapidly, and the pressure-gradient force against self-gravity is weakened, eventually increasing the gas density to above $10\,\mathrm{cm}^{-3}$. On the other hand, the modest change of the temperature seen in the result of the EI scheme does not cause a significant increase in gas density than that of the Crank–Nicholson scheme. Several recipes are proposed to model star formation in simulations of galaxy formation. Commonly, stellar particles are produced as collision-less particles in high-density regions beyond the gas density of the star formation threshold n_{SF}. The result of our simulation shows that the total gas masses for typical star formation thresholds $n_{\mathrm{SF}} > 10\,\mathrm{cm}^{-3}$ and temperature $10^3\,\mathrm{K} < T < 10^4\,\mathrm{K}$ are $1.1\times10^7\,\mathrm{M}_\odot$ and $6.2\times10^6\,\mathrm{M}_\odot$ using the Crank–Nicholson scheme and the EI scheme, respectively. Therefore, this result clearly shows that the overestimation of cooling efficiency in our galaxy collision simulations using the Crank–Nicholson scheme critically affects the formation of galaxies. The numerical accuracy of the radiative cooling plays a significant role in studying galaxy formation precisely.

4 Performance Analysis

4.1 Algorithm Efficiency

We compare the algorithm efficiency of the two schemes. The cooling rate required to calculate the cooling equation is a complicated function of temperature and metallicity and is usually expressed as a numerical table. It is calculated to obtain the cooling rate for any given temperature and metallicity using linear interpolation. The Crank–Nicholson scheme is a second-order implicit scheme, and we use the bisection method for root finding. This method calls for repeated linear interpolation of the cooling rate until a root is found. On the other hand, in the EI scheme, the temporal evolution function is pre-computed before the simulation and is used as a numerical table. Instead of linearly interpolating the

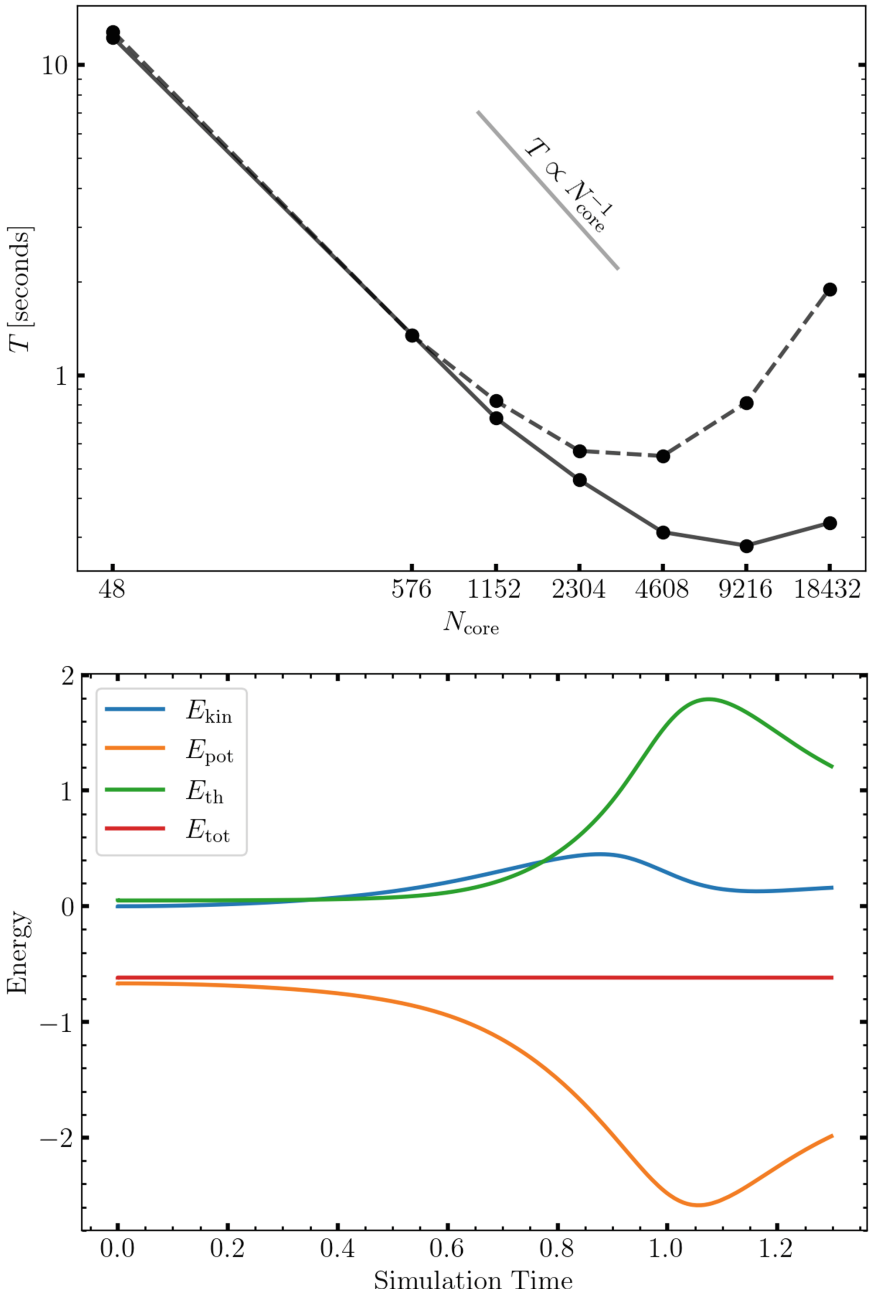

Fig. 5. Top panel: strong scaling for Evrard Collapse Test. The solid black line indicates the scalability with 4 MPI processes and 12 threads per node, and the dashed black line indicates the result with 24 MPI processes and 2 threads per node. The solid gray line represents $T \propto N_{\rm core}^{-1}$. We note that the A64FX processor has 48 cores. Bottom panel: energy evolution in the simulation. Blue, orange, green and red lines are kinetic, potential, thermal, and total energy, respectively. (Color figure online)

cooling rate, the temporal evolution function is calculated using linear interpolation for any given temperature and metallicity. Next, following Eq. (22), the temperature is linearly interpolated for the temporal evolution function after the time step. Therefore, it is clear that the EI scheme is more computationally efficient than the Crank–Nicholson scheme without any loss of accuracy. In addition, parallelization of the EI scheme is straightforward, and no additional difficulties exist because of no communications to other threads.

4.2 Scalability

We investigate the performance of our simulation code using the library of `FDPS` [7,11]. This study is conducted using the FUJITSU Supercomputer Wisteria/BDEC-01 at the University of Tokyo. This supercomputer consists of 7,680 nodes, with an A64FX processor with 48 cores per node. The topology of the network interconnect named TofuD is a 6-D mesh torus with 12 nodes. As a benchmark test, we ran the Evrard Collapse, a gravitational collapse simulation of self-gravitating gas [5]. The initial density distribution of the gas is

$$\rho(r) = \frac{M}{2\pi R^2}\frac{1}{r}\Theta(R-r), \tag{31}$$

where M is the total mass of gas and R is the radius of the gas sphere, and $\Theta(r)$ is the step function. We set $M = R = 1$. The initial velocity is 0 and the initial internal energy is 0.05 GM/R. We measure the elapsed time per time step of each simulation with the number of particles set to 1,099,136. The gravitational softening length is 10^{-5}. The top panel in Fig. 5 shows the strong scaling of this problem using the Wisteria/BDEC-01. We measured the scalability for two types of parallelization, one is the 4 MPI processes and 12 threads per node (solid black line), and the other is 24 MPI processes and 2 threads per node (dashed black line). The bottom panel in Fig. 5 shows kinetic, potential, thermal and total energies as a function of simulation time in the Evrard Collapse. The final energy error in the simulation is about 0.1%.

5 Summary

In this paper, we have investigated the thermodynamic evolution of gas in head-on collisions between dark matter subhalos using one-dimensional analytical models and three-dimensional simulations based on the Exact Integration (EI) scheme by Townsend [19]. We have applied this scheme to define the effective cooling time including temperature dependence of cooling rate. In one-dimensional model, the conventional cooling time is estimated to be shorter than the effective cooling time. We implement the Crank–Nicholson scheme and EI scheme in the gravitational N-body and hydrodynamic simulation code and run the three-dimensional galaxy collision simulations. The results show that the Crank–Nicholson scheme overestimates the cooling efficiency and critically

affects the formation of galaxies. Therefore, to discuss the thermodynamic evolution of the gas properly, it is necessary to take into account the effective cooling time. The scheme impacts the evaluation of radiative cooling in the dense region. Using this scheme has the potential capability to solve the overcooling problem. Finally, we estimate the computational efficiency of the two schemes. The Crank–Nicholson scheme needs iterative calculations to solve the cooling equation, thus linear interpolations must be computed each time. However, the EI scheme requires two linear interpolations to obtain the temperature after a time step. The EI scheme is more computationally efficient than the Crank–Nicholson scheme.

Acknowledgements. Numerical computations were performed with computational resources provided by the Multidisciplinary Cooperative Research Program in the Center for Computational Sciences, University of Tsukuba, Oakforest-PACS operated by the Joint Center for Advanced High-Performance Computing (JCAHPC) and FUJITSU Server PRIMERGY GX2570 (Wisteria/BDEC-01) at the Information Technology Center, The University of Tokyo. This work was supported by JSPS KAKENHI Grant Numbers JP21J21888, JP20K04022.

References

1. Balsara, D.S.: Von Neumann stability analysis of smoothed particle hydrodynamics–suggestions for optimal algorithms. J. Comput. Phys. **121**(2), 357–372 (1995). https://doi.org/10.1016/S0021-9991(95)90221-X
2. Barnes, J., Hut, P.: A hierarchical O(N log N) force-calculation algorithm. Nature **324**(6096), 446–449 (1986). https://doi.org/10.1038/324446a0
3. Barnes, J.E.: A modified tree code: don't laugh; it runs. J. Comput. Phys. **87**(1), 161–170 (1990). https://doi.org/10.1016/0021-9991(90)90232-P
4. Dehnen, W., Aly, H.: Improving convergence in smoothed particle hydrodynamics simulations without pairing instability. Mon. Not. R. Astron. Soc. **425**(2), 1068–1082 (2012). https://doi.org/10.1111/j.1365-2966.2012.21439.x
5. Evrard, A.E.: Beyond N-body: 3D cosmological gas dynamics. Mon. Not. R. Astron. Soc. **235**(3), 911–934 (1988). https://doi.org/10.1093/mnras/235.3.911
6. Gingold, R.A., Monaghan, J.J.: Smoothed particle hydrodynamics: theory and application to non-spherical stars. Mon. Not. R. Astron. Soc. **181**(3), 375–389 (1977). https://doi.org/10.1093/mnras/181.3.375
7. Iwasawa, M., Tanikawa, A., Hosono, N., Nitadori, K., Muranushi, T., Makino, J.: Implementation and performance of FDPS: a framework for developing parallel particle simulation codes. Publ. Astron. Soc. Jpn. **68**(4), 54-1–54-22 (2016). https://doi.org/10.1093/pasj/psw053
8. Lucy, L.B.: A numerical approach to the testing of the fission hypothesis. Astron. J. **82**, 1013–1024 (1977). https://doi.org/10.1086/112164
9. Miki, Y., Umemura, M.: MAGI: many-component galaxy initializer. Mon. Not. R. Astron. Soc. **475**(2), 2269–2281 (2018). https://doi.org/10.1093/mnras/stx3327
10. Monaghan, J.J.: SPH and Riemann solvers. J. Comput. Phys. **136**(2), 298–307 (1997). https://doi.org/10.1006/jcph.1997.5732
11. Namekata, D., et al.: Fortran interface layer of the framework for developing particle simulator FDPS. Publ. Astron. Soc. Jpn. **70**(70) (2018). https://doi.org/10.1093/pasj/psy062

12. Navarro, J.F., Frenk, C.S., White, S.D.M.: The structure of cold dark matter halos. Astrophys. J. **462**, 563 (1996). https://doi.org/10.1086/177173
13. Navarro, J.F., Frenk, C.S., White, S.D.M.: A universal density profile from hierarchical clustering. Astrophys. J. **490**(2), 493 (1997). https://doi.org/10.1086/304888
14. Otaki, K., Mori, M.: The formation of dark-matter-deficient galaxies through galaxy collisions. J. Phys. Conf. Ser. **2207**(1), 012049 (2022). https://doi.org/10.1088/1742-6596/2207/1/012049
15. Prada, F., Klypin, A.A., Cuesta, A.J., Betancort-Rijo, J.E., Primack, J.: Halo concentrations in the standard Λ cold dark matter cosmology. Mon. Not. R. Astron. Soc. **423**(4), 3018–3030 (2012). https://doi.org/10.1111/j.1365-2966.2012.21007.x
16. Springel, V., Hernquist, L.: Cosmological smoothed particle hydrodynamics simulations: the entropy equation. Mon. Not. R. Astron. Soc. **333**(3), 649–664 (2002). https://doi.org/10.1046/j.1365-8711.2002.05445.x
17. Sutherland, R., Dopita, M., Binette, L., Groves, B.: MAPPINGS V: Astrophysical plasma modeling code. Astrophysics Source Code Library p. ascl:1807.005 (July 2018)
18. Sutherland, R.S., Dopita, M.A.: Effects of preionization in radiative shocks. I. Self-consistent models. Astrophys. J. Suppl. Ser. **229**(2), 34 (2017). https://doi.org/10.3847/1538-4365/aa6541
19. Townsend, R.H.D.: An exact integration scheme for radiative cooling in hydrodynamical simulations. Astrophys. J. Suppl. Ser. **181**(2), 391–397 (2009). https://doi.org/10.1088/0067-0049/181/2/391
20. Wendland, H.: Piecewise polynomial, positive definite and compactly supported radial functions of minimal degree. Adv. Comput. Math. **4**(1), 389–396 (1995). https://doi.org/10.1007/BF02123482
21. Zhu, Q., Hernquist, L., Li, Y.: Numerical convergence in smoothed particle hydrodynamics. Astrophys. J. **800**(1), 6 (2015). https://doi.org/10.1088/0004-637X/800/1/6
22. Zhu, Q., Smith, B., Hernquist, L.: Gas cooling in hydrodynamic simulations with an exact time integration scheme. Mon. Not. R. Astron. Soc. **470**(1), 1017–1025 (2017). https://doi.org/10.1093/mnras/stx1346

Open Access This chapter is licensed under the terms of the Creative Commons Attribution 4.0 International License (http://creativecommons.org/licenses/by/4.0/), which permits use, sharing, adaptation, distribution and reproduction in any medium or format, as long as you give appropriate credit to the original author(s) and the source, provide a link to the Creative Commons license and indicate if changes were made.

The images or other third party material in this chapter are included in the chapter's Creative Commons license, unless indicated otherwise in a credit line to the material. If material is not included in the chapter's Creative Commons license and your intended use is not permitted by statutory regulation or exceeds the permitted use, you will need to obtain permission directly from the copyright holder.

